THE INTERFACE MIXING LAYER AND THE TIDAL DYNAMICS AT THE EASTERN PART OF THE STRAIT OF GIBRALTAR.

1.- Introduction

The large velocities, their vertical shear and, particularly, the important tidal currents that interact with a very constraining bathymetry distort the conceptual model of a two-layer exchange of homogeneous Mediterranean and Atlantic waters through the strait of Gibraltar. A more realistic scenario must include an interface layer of mixed water, which feeds with water from both layers, in which water properties change gradually from Atlantic to Mediterranean values. It is often omitted in theoretical and experimental works aimed at investigating the most relevant aspects of the internal dynamics such as the hydraulic control exerted on the exchange (Armi and Farmer, 1985, 1988; Bryden et al., 1994; Garcia Lafuente et al., 2002a,b). However the simple two-layer model is unable to explain a few relevant aspects dealing with mixing and entrainment of water and biologically-related processes. It also fails to explain more sophisticated features of the hydraulic control that have been observed (Sannino et al. 2007, 2009).

One of the first attempts to include the interface layer in the dynamics of the exchange was made by Bray et al. (1995), who showed that this layer contributed to the inflow east of Camarinal sill (CS, see Fig. 1) and to the outflow west of CS. They also showed that the layer increased its thickness as we move away from CS in both directions. Tides were not discussed in their conceptual model. Other recent works (Sannino et al., 2007, 2009; Sánchez Garrido et al., 2011) included the interface layer to extend the two-layer hydraulic theory to the case of three layers in order to explain the persistence and/or intermittency of hydraulic control in key sections of the Strait that cannot be properly addressed in the simpler two-layer exchange.

The interface layer is of relevance for biology. Echevarría et al. (2002) analyzed their role in the biological processes that take place within the dimensions of the strait of Gibraltar. They pointed out the importance of internal, tidally-driven features such as the internal hydraulic jump formed leeward of CS to supply energy for mixing and, hence, to originate and maintain the interface layer, an issue further investigated by Macias et al., (2007). Echevarría et al. (2002) showed that the depth and thickness of the interface layer have along-strait structure, being shallower at the eastern part of the Strait where it is associated with peak values of chlorophyll fluorescence (Macias et al. 2005), and also cross-strait structure due to the Earth rotation, which cannot be ignored as the internal Rossby radius of deformation is comparable to the width of the strait. García Lafuente et al. (2000) showed that both parameters, depth and thickness, are markedly modulated by tides at the eastern part of the strait and Macias et al. (2006) extended this modulation to the flux of phytoplankton biomass into the Alboran Sea, which, according to these authors, exhibits a pulsating pattern.

From a biological point of view the upward sloping of the interface layer to the east introduces an important asymmetry between the western and eastern halves of the strait. In relatively large portions of the eastern half the layer is shallow enough to expose the nutrient-enriched waters to the sun radiation in the photic zone and enhance primary production. Since finally this layer enters the Mediterranean Sea, it can contribute to the water enrichment of the north-western sector of the Alboran Sea (Macías et al. 2007, 2008; Vazquez et al. 2009), although the contribution of this process to the total productivity of the area is still a subject of ongoing research.

From a physical point of view, the eastern half of the strait is also more appealing than the western half since it is systematically swept by large-amplitude internal wave (LAIW, hereinafter) trains that originate in CS after the release of the hydraulic jump periodically formed leeward of the sill (Armi and Farmer, 1988; Vazquez et al., 2009; Sanchez-Garrido et al, 2011) and radiates finally into the Mediterranean Sea. LAIWs have been linked to biological activity because their potential for mixing waters and further enrichment of the interface and surface layers (Macias et al. 2007, 2008; Vazquez et al. 2009). All these reasons have motivated the election of the eastern half of the strait as the target area of our study, which is carried out using the numerical simulations of a non-hydrostatic version of the Massachusetts Institute of Technology general circulation model, (MIT-gcm, Marshall et al, 1997a,b). It is worth noting that this model has been already used to reproduce successfully the generation, evolution and propagation of LAIWs in the strait of Gibraltar (Sánchez-Garrido et al., 2011).

The objective of this paper is the comprehensive description of the dynamics of the interface layer at tidal time-scales in the target area and its likely connections with biological processes using a high spatial resolution numerical model. To this aim the paper has been organized as follows. Next Section 2 presents a short summary of the numerical model, Section 3 describes the spatial-temporal behavior of interface layer in the eastern part of the strait, Section 4 addresses the different processes that contribute to the interface dynamics while Section 5 describes likely biological connections of the interface dynamics. Section 6 summarizes our conclusions.

2.- Numerical model

The MIT-gcm solves the fully non-linear, non-hydrostatic incompressible Navier- Stoke equations under Boussinesq approximation for an incompressible fluid with a spatial finite-volume discretization on a curvilinear computational grid. The model is described in detail by Marshall et al. (1997a, 1997b) and in the MITgcm Group Website http://mitgcm.org/sealion/online_documents/node2. Its adaptation to the bathymetry of strait of Gibraltar and surrounding basins can be seen in Sánchez-Garrido et al. (2011). A short overview is given next.

The model domain, covering part of the Alboran Sea and the Gulf of Cadiz, is horizontally discretized with a very fine resolution curvilinear grid with Δx~50m and Δy~200m within the Strait and 53 vertical levels with vertical step Δz~7.5m in the upper 300 m, that gradually increases towards the bottom. The bottom topography has been obtained by merging the ETOPO2 bathymetry (NOAA, 2006) with the high resolution bathymetric chart of the Strait of Gibraltar by Sanz et al. (1991).

The parametrization of sub-grid scale mixing and dissipation is carried out following the turbulent closure schemes by Pacanowski and Philander (1981) in the vertical and Leith (1968) in the horizontal diffusivity.

Initial conditions for temperature and salinity were obtained from Medar-MedAtlas Database [MEDAR Group, 2002] for the climatological month of April. The mean two-way exchange is obtained by laterally forcing the model through the imposition of the mean baroclinic velocities and tracers extracted from the intermediate resolution model developed by Sannino et al. (2009) to study the water exchange through the Strait of Gibraltar and its hydraulic behavior. The model is run with this configuration for a spin-up period of 11 days, after which a quasi-steady circulation is observed. In a second step the tidal forcing is introduced by laterally forcing the model with the main diurnal (O1, K1) and semidiurnal (M2, S2) barotropic tidal velocities from DONDE?.. The simulation was then extended through a second spin-up period of 11 days in order to attain a stable time-periodic solution. One month of this final solution constitutes the numerical dataset of this study. This same dataset has been already compared successfully with observations in Sanchez-Garrido et al (2011) who made use of them in their study of LAIWs in the strait of Gibraltar.

3.- The tidal behavior of the interface layer

3.1 Definition of the interface layer thickness and position

The required upper and lower boundaries of the interface layer have been computed according to the procedure described in Sannino et al. (2007, 2009). The method fits the vertical profiles of salinity, which is the hydrological variable that makes the greatest contrast between Atlantic and Mediterranean waters, to a hyperbolic tangent function. The depths at which the straight line passing through the flex point of the fitted curve intersects the vertical lines passing through the surface and bottom salinity are taken as the upper and lower boundaries, respectively and determine the layer thickness (see sketch in Fig. 2e). The mean position of the interface is defined as the depth of the mid-point of the interface layer.

3.2 Semidiurnal evolution of the interface layer

Figure 2 shows three snapshots showing the time evolution of the interface layer along the west-east vertical section of the strait axis indicated in Figure 1. The time of each plot, referred to the barotropic tidal current, is depicted in Figure 2d. The first panel

(Fig. 2a) coincides with the peak of westwards tidal current[1] and illustrates the formation of the internal hydraulic jump over CS. At this time the interface layer east of CS is very thin and relatively shallow (two properties that are linked to each other, see Fig. 3 and comments below), while west of CS it is much deeper and noticeably thicker. This asymmetry is a recurrent feature in the strait dynamics as pointed out by Sanchez Román et al., (2012). Further east the thickness of the layer increases in the wake of the LAIWs' train that appears at the left of the panel progressing to the east. Figure 2b corresponds to the beginning of the ebb tide (one hour after slack tide, Fig. 2d); at this time the hydraulic jump has been already released and progresses eastwards while disintegrating in LAIWs (see Sánchez-Garrido et al., 2011). The interface layer in front of the LAIWs remains very thin and moves with the wave train. Figure 2c, which corresponds to the peak of ebb current (Fig. 2d), shows the LAIWs train of the previous snapshot about emerging into the Mediterranean Sea and leaving a very thick and relatively deepened interface layer behind, which contrasts with the much thinner layer west of CS at this time (the already mentioned asymmetry).

There may be several physical processes involved in the local shrinking and stretching of the interface layer in the eastern part of the strait. It can be thickened by local mixing, the LAIWs being a likely energy supply mechanism, by entrainment of water from the underlying Mediterranean and/or from the overlying Atlantic layers[2] and also by horizontal advection of mixed waters during the ebb tide: during the flood tide, Atlantic and Mediterranean waters are strongly mixed in TB at the supercritical-to-subcritical flow transition downstream of the internal hydraulic jump formed over CS (Figure 2a,

---

[1] We shall refer the west-going phase of the barotropic tidal currents as the flood tide since it corresponds to the raising phase of sea level (García Lafuente et al., 1990). Ebb tide will correspond to eastward barotropic tidal current.

[2] The mean vertical profile of along-strait velocity decreases with depth for which Atlantic surface layer moves faster than the interface layer. As far as we focus on the interface layer, water coming from above would be said "detrained" rather than "entrained". Nevertheless we will maintain "entrainment" for simplicity throughout this study.

Armi and Farmer, 1988; Sanchez-Garrido et al., 2011; García Lafuente et al., 2011), where Wesson and Gregg (1994) found peak values of dissipation rates in excess of 10^{-2} Wkg^{-1}, which are orders of magnitude greater that the typical values in the interior ocean. After the release of the jump near high tide, a considerable volume of these mixed water will progress eastwards in the wake of the LAIW's train.

None of these three processes can re-stratify the water column and make the interface layer thinner. Figure 3 shows that the flood tide is the physical process responsible for the re-stratification since the depth and thickness diminish progressively during the negative phase of the current (flood) in the Mediterranean layer in the eastern half of the strait and reach their minimum about the time this current vanishes. The process is forced by the internal hydraulics of the strait: during the flood tide the hydraulic control in CS prevents all the Mediterranean water forced westwards by the tide from crossing the sill (Sanchez-Román et al., 2012) and a considerable volume remains accumulated in the eastern half of the strait. This pool of Mediterranean water pushes the overlying layers upwards converting kinetic into potential energy and bringing the interface layer both towards the surface and to its minimum thickness. Hence the good positive correlation found between these variables (r^2~0.6 on average at lag~0 at the different sections showed in Figure 1).

3.3 Spatial-temporal variability of the interface layer

Figures 4a and 4b show the time evolution of the interface layer at sites "a" and "b" in the axis of the strait (see Fig. 1). The inserts in the panels highlight the semidiurnal periodicity of the interface thickness fluctuations, which are far from being sinusoidal, in agreement with the time-space evolution sketched in Figure 2.

The interface thickness shows a spring-neap modulation being locally thicker and with greater range of semidiurnal oscillations in spring tides, as expected. The diurnal inequality is clearly distinguishable during the neap-tide period (days 20-27), a result that stems from the relatively high importance of diurnal tidal currents that becomes more evident during neap tides (Fig. 4c). The inequality has noticeable influence on the formation and release of the hydraulic jump over CS (Armi and Farmer, 1988) and, hence, on the apparition of LAIW trains in the eastern strait (Watson and Robinson, 1990; Sanchez Garrido et al., 2008), which in turn affects the thickness of the interface layer (Fig. 4a and 4b).

In addition to time-variability, the interface layer also shows spatial structure. Regardless the neap-spring cycle, the interface mean thickness increases to the east while its range of semidiurnal oscillation decreases. Semidiurnal periodicity also fades out in this direction (compare inserts in Fig. 4a and 4b) and it tends even to disappear towards the east during neap-tides (Fig. 4b).

Shaded contours of Figure 5 summarize the spatial-temporal evolution of the interface thickness along the central axis of the strait. Most of the above described features are easily identifiable such as, for instance, the thickening (on average) of the interface layer towards the east or the very clear semidiurnal signal and diurnal inequality east (but close) to CS which fades out to the east.

The behavior of the interface thickness downstream (to the west) of ES and CS deserves particular attention. The deep grey shading located at 5.8ºW west of CS is linked to the internal hydraulic jump or, more specifically, to the supercritical-to-subcritical flow transition downstream the jump in TB. When the jump is released, the deep grey shading (interface thickening) progresses eastwards leaving a rather stratified water column (light grey) at this location (5.8ºW), which eventually thickens by many meters in the next tidal cycle. On the contrary, at ES the interface thickness is within the range 50-70m all the time and no progression to the east is observed. All this suggests that the hydraulic control over ES is much more permanent than over CS, as put forward by Sannino et al., (2007, 2009) and Sanchez Román et al., (2009). Notice also that the thickening of the interface in the supercritical-to-subcritical transition downstream ES shows little tidal modulation as compared to the transition downstream CS.

The deep grey contours west and east of CS in Figure 5 tend to be aligned along straight lines of negative and positive slope, respectively (see white lines). In this time-space diagram the slope is indicative of the velocity at which the disturbances propagate, which is readily estimated (values beside the lines). East of the sill, three regions of different positive slope can be distinguished: the first one runs from around 5.8ºW, where strong mixing takes place in the flow transition, to a few distance east of CS (velocity 0.3 ms^{-1}); the second one goes from this point to GC suggesting a disturbance speed of around 2 ms^{-1} and the third one is eastwards of GC where the strait opens into the Alboran Sea (see Figure 1) and the speed decreases to 0.6-0.7 ms^{-1}. West of CS, within the Tangier basin, the disturbance propagates at around -1 ms^{-1}, the negative sign meaning westwards propagation. Since all these disturbances have tidal origin, the time-space diagram confirms the fact that the strong internal tide observed in the strait of Gibraltar is generated at CS from where it radiates in both directions.

4.- Processes involved in the interface dynamics.

Several processes have already been invoked to explain the thickening and subsequent thinning of the interface along the tidal cycle. All they are addressed next

4.1 Horizontal advection from Tangier basin.

A lagrangian experiment in which inert particles (passive tracer) were abandoned in the Tangier basin was performed to assess the impact of horizontal advection in the interface dynamics east of CS. The temporal evolution of the tracer follows the same advection–diffusion equation as temperature and salinity

$$\frac{\partial C}{\partial t} = -\mathbf{u} \cdot \nabla C + \nabla \cdot k \nabla C \qquad [1]$$

where C is the tracer concentration, **u** is the velocity vector, and k is the diffusion tensor. Convection and various advanced mixing schemes can be formulated into three-dimensional tensors in the form of [1] (Cushman-Roisin and Beckers, 2011).

Initially the passive tracer is homogeneously distributed in the interface layer in TB with a concentration of 1 ítem m^{-3} (Fig. 6a). Time origin is the slack (barotropic) tide at CS corresponding to high tide (insert in Fig. 6h). By this time the internal hydraulic jump has already been released (it does ~ 2 h before high tide) and the bore has moved ~6 km eastwards of CS (green-shaded bar on top of panel 6a) showing up an incipient LAIWs train behind. The simulation goes on for a period of 36 hours (Fig. 6h).

Starting with the ebb tide (Fig. 6a, 6b and 6c), the nose of the mixed water advected from TB is left behind the front of LAIWs by an increasing distance (see the length of the red-shaded bars on top of panels 6a, 6b and 6c). It is straightforward to compute the LAIWs front speed relative to the nose: it does at a mean speed of 0.75 m s^{-1} between t=0h (Fig. 6a) and t=3h (Fig. 6b), and at 0.65 m s^{-1} between t=3h (Fig. 6b) and t=7h (Fig. 6c). However the rear of the LAIWs train and the nose separate at a relative speed of ~0.3 m s^{-1} (green-shaded bars on top of the panels), which is roughly half the relative speed at which the LAIWs front progresses. This is due to the continuous generation of new waves that incorporate at the rear and lengthen the LAIWs train as it proceeds to the east (compare Fig. 6b and 6c for instance; see also Vlasenko et al. (2009) and

Sánchez-Garrido et al. (2011)). During the flood tide (Fig. 6d) the advection is partly stopped, some water in the interface is forced oceanwards while the interface itself shallows and becomes thinner. Figures 6e to 6h show the further evolution of the tracer remains injected at t=0 that has not abandoned the strait yet (no new tracer was injected in TB basin in the successive two tidal cycles, note the different color scale). The pale green-yellow colors extending across the interface layer in Figures 6g and 6h suggest diapycnal diffusion and this fact along with the thickening of the interface between the nose of the passive tracer and the rear of the LAIWs in Figures 6b and 6c suggest that advection of water from TB is not the only mechanism acting to thicken the interface.

4.2 Water entrainment

Dealing with a layered model, entrainment is a useful tool. The sketch of Figure 7A illustrates the procedure followed to estimate the entrained water. It represents a finite volume V bounded by fixed cross-strait sections, which will be eventually identify with the sections in Figure 1, and by two isohalines of given values, whose depth change with time. Isohalines S_A=36.3 and S_M=38.1 have been selected as upper and lower bounds, respectively, as they are the surfaces that better coincide with the boundaries of the interface layer defined in Section 3.1 in the eastern half of the strait.

Continuity and salt conservation equations in this control volume will be written as

$$\frac{dV}{dt} = \sum_k Q_k \qquad [2\text{-a}]$$

$$\frac{dS}{dt} = \sum_k QS_k \qquad [3\text{-a}]$$

where Q_k and QS_k are the net flow and salt flux into the control volume, respectively, and V and S are the water volume and salt content in the interior. At tidal time-scale the isohalines are forced to undertake large vertical oscillations, implying large fluctuations of V and S and of their time derivatives. Figure 7b shows the time evolution of $Q_2(t)$ and

$Q_3(t)$ and their difference, which is the major contributor to dV/dt in [2-a] since vertical advection must be much less than horizontal advection. The difference shows a noticeable tidal periodicity indicative of the periodic thickening and slimming of the interface layer, which is also evidenced by the solid line in Figure 3. In the long term however (i.e., averaging over several tidal cycles) the interface thickness must be locally stationary and, therefore, $dV/dt=dS/dt=0$. The time average of equations [2-a] and [2-b] thus reduce to (using the convention of Figure 7a)

$$Q_{i+1} - Q_i = QA_{ei} + QM_{ei} \qquad [2\text{-b}]$$

$$QS_{i+1} - QS_i = QAS_i + QMS_i \qquad [3\text{-b}]$$

where Q_i is the flow of the interface layer through section i computed directly from the model output, QA_{ei} and QM_{ei} are the flows of entrained water from the upper (Atlantic) and lower (Mediterranean) layers that enters (positive sign) or exits (negative sign) the control volume between sections i and $i+1$, QS_i is the salinity transport through section i computed from the model, and QAS_i and QMS_i are the salinity transport through the upper and lower boundary associated with the entrained flows. The salinity transports QAS_i and QMS_i can be approached by

$$QAS_i = QA_{ei}S_A, \quad QMS_i = QM_{ei}S_M \qquad [4]$$

where $S_A=36.3$ and $S_M=38.1$ are the salinities of the upper and lower isohalines of the control volume. From equations [2-b] [3-b] and [4], entrained waters are obtained as

$$QA_{ei} = \frac{(Q_{i+1} - Q_i)S_M - (QS_{i+1} - QS_i)}{S_M - S_A} \qquad [5]$$

$$QM_{ei} = \frac{(QS_{i+1} - QS_i) - (Q_{i+1} - Q_i)S_A}{S_M - S_A} \qquad [6]$$

Figure 7c shows QAe_i and QMe_i in the 5 boxes defined by the six cross-strait sections of Figure 1. Water entrained from above, QAe_i, is rather similar in the different boxes (around 0.025 Sv/box, light grey triangles in Fig. 7c) while QMe_i is less homogeneous, showing negative values in two out of five boxes, especially in the first one (light grey inverted triangles in Fig. 7c). More interesting is the cumulated entrained water shown by the thick triangles: in both cases it contributes positively to increase the flow through the interface layer between sections 1 and 6. Curiously, the contribution of the upper Atlantic layer is about twice that of the lower Mediterranean layer suggesting that the progressive thickening of the interface towards the east is mainly due to the incorporation of fresher water from the surface layer.

Figure 7d is the scatter plot of the entrained water versus the vertical shear. It has been computed as the velocity difference between z=3m (the surface level) and the depth of S=36.8 divided by the variable depth difference between both levels, and provides an estimation of the shear in the upper boundary of the interface layer. Similarly, the velocity difference between S=37.7 and z=250m divided by the distance between these levels has been used as an indicative of the shear at the lower boundary of the interface. Except for the water entrained through the bottom boundary of box 1 (symbol 1B in Figure 7d) the rest of the dots lay reasonably close to the fitting line (dashed line) suggesting the linear relationship between entrainment and shear often used in layered models (Gerdes et al., 2002, Nielsen et al, 2004). The anomalous behavior of dot 1B is surely due to the proximity of box 1 to CS, where the assumed lower interface boundary of S=38.1 includes a large portion of west-moving water column inside the interface layer that implies negative entrainment, as actually found in this box.

4.3 Mixing by internal waves

Figure 8 shows two salinity profiles at sites “a” and “b” of Figure 1 after the LAIW train has passed by. The vertical salinity gradient is smoother at site “b” suggesting that the halocline (and hence the pycnocline) is eroded as the thickening of the interface progresses to the east. Water entrainment would explain partially the erosion but this mechanism would act preferably near the top and bottom of the interface layer leaving the middle part rather unaltered, but Figure 8 shows that this does not seem to be the case.

Another already mentioned mechanism that has not explored been yet is the mixing potential of the progressing LAIW trains. Left panels of Figure 9 depicts three situations of the generation and propagation of LAIWs whereas right panels present the gradient Richardson number Ri computed at 160m depth, which is roughly the depth of the middle part of the interface layer as suggested by Figure 8. Very low values of Ri are found at the rear part of the progressing LAIWs packet that would facilitate and propitiate shear instabilities, supporting the hypothesis that LAIWs contribute to the mixing in the interior of the interface layer . It is also worth mentioning the extended very low values of Ri in TB observed in Figure 9d. At this time no traces of LAIWs are observed and the roughness of the sea surface over and westwards of CS is the only remarkable signature of the internal dynamics (Figure 9a), which in turn suggests that the hydraulic jump is formed or being formed and that its formation is accompanied by strong mixing within that basin.

5.- Biological connections of the interface dynamics

The previous section has identified some mechanisms associated with the tidal dynamics through which the interface layer in the target area might be nutrient-enriched and brought up to the photic layer. Some of them have obvious implications on the biological productivity and deserve a more detailed analysis and discussion.

5.1 Horizontal advection.

Horizontal advection is an important process regarding the enrichment of the interface layer, as discussed in section 4.1. The huge mixing in TB during the flood tide (Figure 9d) makes the mixed and, therefore, nutrient enriched waters available for eastwards advection during the ebb tide. There is however the possibility that the enriched waters were injected from the coastal areas into the main channel of the strait as hypothesized by Vazquez et al. (2009) and Bartual et al. (2011).

A new experiment was carried out to address this point. Passive tracers were injected with homogeneous concentration in the middle part and in the coastal areas of the strait at the locations shown in Figures 10a and 10e, respectively. The experiment started (t=0) shortly before the slack-tide corresponding to high tide (bottom panel of Figure 10), when the hydraulic jump is about being released, and run for 36 hours. The time origin has been intentionally selected since it coincides with the starting time of the remarkable horizontal advection of interface waters to the east (Section 4.1, Figure 6). Panels in Figure 10 show the subsequent evolution of the vertically integrated concentration for the initial situations depicted in Figures 10a and 10e..

The tracer abandoned in the mid-channel within TB (Figure 10a) is advected in both directions by the joint action of the mean exchange and the tidal forcing. It quickly adopts an elongated shape that outlines the main axis of the channel without intruding the coastal areas. At the end, it flows out through both open boundaries of the basin. The west-going branch flows at depths greater than the height of the MB seamount (Figure 1), which appears clearly shaped in Figures 10b to 10d as the outflowing water splits to skirt its pronounced topography. The branch flowing through the east remains basically in the central part of the channel although it approaches the shores as the strait narrows. Finally, it enters the Alborán Sea following an expected east-northeast oriented pathway (Figures 10c and 10d).

The coastal waters initially close to the northern shore at the western part of the strait (Figure 10e) are advected in both directions by the changing tide but they remain attached to the shore (Figures 10f to 10h). Cross strait injection into the main channel, if any, is negligible. Something similar happens to the coastal waters located initially in the south, although there are two remarkable differences: they are advected eastwards preferably (Figure 10g, 10h) and a non-negligible portion detaches from the southern shore and reaches the middle part of the channel by the eastern end of the strait (Figure 10g). They would join the waters flowing along the main channel (Figure 10d) and contribute to the tracer advection towards the interior of the Alborán Sea. Nevertheless, most of the original water turns right as they exit the strait and remains close to the African shore (Figure 10h), featuring an spatial pattern that recalls the MERIS image of Figure 2 in Vazquez et al. (2009) very much.

5.2 Residence time

The former numerical experiment has shown that the mixed water in the interface layer produced within TB and visualized by the tracer concentration leaves the strait through both open boundaries but it takes some time to do it. Figure 11 presents the evolution of the tracer percentage and shows that, after 36 hours (~ three tidal cycles), around 60% has flown out of TB to the Atlantic ocean through ES, 30% has already crossed CS to the east (Mediterranean) and only 10% remains still in the basin. Notice that the very initial partition of the percentages depend on the time origin of the experiment: the quick increase of the east-going tracer (to the Mediterranean sea) observed in Figure 11 results from the fact that *t*=0 nearly coincides with the beginning of the ebb current (bottom panel of Figure 10). Later on the percentage decreases and remains oscillating slightly around the mentioned value of 30%.

While the mixed waters flowing west are too much deep to contribute to the primary production (depths >200m, see Figure 6), the interfacial waters flowing eastwards are inside a shallower layer within the reach of the sun radiation and, in addition, they are brought closer to the surface periodically by the tidal dynamics. Therefore they have potential to support local primary production. The time that the interface waters mixed in TB by the hydraulic jump and the related flow transitions remain within the dimensions of the strait but eastwards of CS is not easy to determine because the vertical shear of the currents and the low frequency tidal variability (spring-neap cycle). Judging from panels in Figures 6 and 10, it could be estimated between two and three tidal cycles.

6.- Conclusions

The tidal dynamics of the interface layer in the eastern part of the strait shows a complex pattern that involves different physical processes. Interface thickness and depth have been used to analyze their periodic evolution since both variables have been shown to exhibit such tidal variability (García-Lafuente et al, 2000; Echevarría et al, 2002). The thickening phase begins with the release of the internal hydraulic jump formed over CS during the flood tide, which indicates that horizontal advection is a fundamental ingredient of the interface dynamics but is not the only one. The simple budget computation illustrated in Figure 7a shows that there is tide-average water entrainment from the overlying (Atlantic) and underlying (Mediterranean) layers that increase by a factor of 2 the volume transport within the interface layer in the eastern strait (Figure 7b) of which 2/3 is entrained from above and 1/3 from below. Since nutrient source is the deep ocean, entrainment is of limited relevance in order to enrich the interface in the eastern part of the strait. Entrainment would erode the salinity (hence density) vertical gradient of the interface but the low values of the Richardson number found in the rear of the LAIWs train (Figure 9) around the midpoint of the interface layer suggest that internal waves contribute noticeably to the dyapicnal mixing in the interface interior.

All the three processes above act together to explain the thickening phase of the interface. None of them can explain its periodic thinning, obviously. It is the flood phase of the tide acting on the lower Mediterranean layer at the eastern part of the strait along with the topographical and hydraulic constriction imposed by the sill of Camarinal that raises and makes the interface thinner, forcing the pre-existing interface water to move towards both ends of the strait. Thus interface water must enter the Alborán Sea as successive periodic pulses modulated by tides in a manner that recalls the pulsating events cited by Macias et al. (2006).

Other numerical experiments aimed to investigate biological-related issues have been performed. One of them addressed the question raised by previous studies about the possibility of injection of coastal waters into the main vein of the Atlantic inflow that would contribute to its biological enrichment (Vazquez et al., 2009; Bartual et al., 2011). Our results (Figure 10) indicate that, to a limited extent, such injection could take place from the southern shore but not from the northern one where the tracers remain attached to the shore until it enters the Alborán Sea.

Other biologically-relevant issue is the time interval that interface waters reside within the strait dimensions because the interface layer in the eastern strait is exposed to the sun radiation, which makes local primary production feasible. The same numerical experiment allowed us to make an estimation of two to three tidal cycles for this interval once the mixed and nutrient-enriched waters in TB are released by the loss of the hydraulic control at CS. This relatively small residence time will be still shortened by the fraction corresponding to nighttime and by the eventual deepening of the interface beyond suitable radiation levels, all which suggests that local primary production, if any, must be very limited. To this respect, some MERIS images showing cross-strait oriented bands of chlorophyll that depict the internal wave fronts (see for instance Figure 2 of Vazquez et al., 2009), would lead to the misleading conclusion of local primary production associated with LAIWs. More probably, however, the chlorophyll has been advected from TB during the previous ebb and the observed pattern is the result of its redistribution by the LAIWs velocity field of the next ebb in the manner illustrated by Figure 6g.

Another indirect but yet interesting conclusion from this experiment is the sharing of interface waters between inflow and outflow. Tangier basin is the key place for sustained mixing to form the interface and these mixed waters are drained eastwards and westwards flowing across the main sills that bound the basin. Figure 11 shows that the sharing is in the proportion 2:1 for the outflow, indicating that the interface layer generated in TB is mainly evacuated by the outflow. The incorporation of this mixed water to the outflow represents the first step of the erosion of Mediterranean water properties in the Atlantic Ocean and its effect is already distinguishable in ES, as shown by García-Lafuente et al., (2011).

The model does not include the wind effect over the surface water nor the remote forcing driven by atmospheric pressure variations over the Mediterranean basin (García Lafuente et al, 2002a,b), which may be important agents to distort the periodic tidal pattern (Vazquez et al., 2008) and, hence, to affect some of our conclusions. Among them one particularly sensitive is the injection of coastal waters into the center of the channel, which can be easily carried there by cross-strait Ekman transport (north-to-south by westerlies, south-to-north by easterlies), explaining the presence in the middle channel of chlorophyll with the same characteristics as coastal chlorophyll that was found by Macias et al. (2008).

Acknowledgments

References

Armi, L., and D. M. Farmer (1985), The internal hydraulics of the Strait of Gibraltar and associated sill and narrows, Oceanol. Acta, 8, 37–46.

Armi, L., and D. M. Farmer (1988), The flow of Atlantic Water through the Strait of Gibraltar, Prog. Oceanogr., 21(1), 1–105.

Bartual, A., D. Macías, A. Gutierrez-Rodriguez, C.M. García, and F. Echevarría (2011), Transient pulses of primary production generated by ondulatory processes in the western sector of the Strait of Gibraltar. J. Mar. Syst. 87, 25–36, doi:10.1016/j.jmarsys.2011.02.021.

Bray, N.A., J. Ochoa, and T.H. Kinder (1995), The role of interface in exchange through the Strait of Gibraltar. J. Geophys. Res., 100 (C6), 10755–10776.

Bryden, H. L., J. Candela, and T.H. Kinder (1994), Exchange through the Strait of Gibraltar, Prog. Oceanogr., 33, 201-248.

Cushman-Roisin, B., and J.M. Beckers, Introduction to Geophysical Fluid Dynamics. Physical and numerical aspects. Academic Press, Massachusetts, USA, 828 pp.

Echevarría, F., J. García Lafuente, M. Bruno, G. Gorsky, M. Goutx, N. González, C.M. García, F. Gómez, J.M. Vargas, M. Picheral, L Striby, M Varela, J.J. Alonso, A. Reul, A. Cozar, L. Prieto, T. Sarhan, F. Plaza, and F. Jiménez-Gómez (2002), Physical-biological coupling in the Strait of Gibraltar, Deep-Sea Res., 49, 4115-4130.

García Lafuente J., J.L. Almazan, F. Fernandez-Castillejo, A. Kribeche, A. Hakimi (1990), Sea level in the Strait of Gibraltar: tides. Int. Hydrogr. Rev., LXVII(1), 111-130.

García Lafuente J., J.M. Vargas, F. Plaza, T. Sarhan, J. Candela, B. Basheck (2000), Tide at the eastern section of the Strait of Gibraltar. J. Geophys. Res. 105:14197–14213, doi:10.1029/2000JC900007.

Garcia Lafuente, J., J. Delgado, and F. Criado-Aldeanueva (2002a), Inflow interruption by meteorological forcing in the Strait of Gibraltar. Geophys. Res. Lett., 29 (19), 1914, doi:10.1029/2002GL015446.

García Lafuente, J., E. Alvarez Fanjul, J. M. Vargas, and A. W. Ratsimandresy (2002b), Subinertial variability in the flow through the Strait of Gibraltar, J. Geophys. Res., 107(C10), 3168, doi:10.1029/2001JC001104.

García Lafuente, J., A. Sánchez-Román, C. Naranjo, J.C. Sánchez-Garrido (2011), The very first transformation of the Mediterranean outflow in the Strait of Gibraltar, J. Geophys. Res., 116, C07010, doi:10.1029/2011JC006967.

Gerdes, F., C. Garrett, and D. Farmer (2002), On internal hydraulics with entrainment. J. Phys. Oceanogr., 32, 1106-1111.

Leith, C.E. (1968), Diffusion approximation for two-dimensional turbulence, Phys. Fluids, 10, 1409–1416, 1968.

Macías, D., C.M. Garcia, F. Echevarria, A. Vazquez-Escobar, and M. Bruno (2006), Tidal induced variability of mixing processes on Camarinal Sill (Strait of Gibraltar). A pulsating event. J. Mar. Sys., 60, 177-192, doi:10.1016/j.jmarsys.2005.12.003

Macías, D., A.P. Martin, J. García Lafuente, C.M. García, A. Yool, M. Bruno, A. Vázquez, A. Izquierdo, D. Sein, and F. Echevarría (2007), Mixing and biogeochemical effects induced by tides on the Atlantic–Mediterranean flow in the Strait of Gibraltar. An analysis through a physical–biological coupled model. Prog. Oceanogr. 74, 252–272, doi:10.1016/j.pocean.2007.04.006.

Macías, D., L.M. Lubian, F. Echevarría, E. Huertas, and C.M. García (2008), Chlorophyll maxima and water mass interfaces: tidally induced dynamics in the Strait of Gibraltar. Deep-Sea Res., I, 55, 832-846, doi: .

Marshall, J., A. Adcroft, C. Hill, L. Perelman, and C. Heisey (1997a), A finite-volume, incompressible Navier Stokes model for studies of the ocean on parallel computers. J. Geophys. Res, 102 (C3), 5753-5766, doi:10.1029/96JC02775.

Marshall, J., C. Hill, L. Perelman, and A. Adcroft (1997b), Hydrostatic, quasi-hydrostatic, and nonhydrostatic ocean modeling. J. Geophys. Res, 102(C3), 5733-5752, doi:10.1029/96JC02776.

MEDAR Group (2002), Medatlas 2002: Mediterranean and Black Sea Database of Temperature, Salinity and Bio-Chemical Parameters Climatological Atlas, Eur. Comm. Mar. Sci. and Technol. Programme, Paris.

Nielsen, M.H., L. Pratt, and K. Helfrich (2004), Mixing and entrainment in hydraulically driven stratified sill flows. J. Fluid Mech., 15, 415-443

Pacanowski, R.C., and S.G.H. Philander (1981), Parameterisation of vertical mixing in numerical models of tropical oceans, J. Phys. Oceanogr., 11, 1443–1451.

Sánchez Garrido, J. C., J. García Lafuente, F. Criado Aldeanueva, A. Baquerizo, and G. Sannino (2008), Time-spatial variability observed in velocity of propagation of the internal bore in the Strait of Gibraltar, J. Geophys. Res., 113, C07034, doi:10.1029/2007JC004624.

Sánchez-Garrido, J.C., G. Sannino, L. Liberti, J. García Lafuente, and L. Pratt (2011), Numerical modelling of three-dimensional stratified tidal flow over Camarinal Sill, Strait of Gibraltar, J. Geophys Res, 116 , C12026, doi:10.1029/2011JC007093.

Sánchez-Román, A., G. Sannino, J. García Lafuente, A. Carillo, and F. Criado-Aldeanueva (2009), Transport estimates at the western section of the Strait of Gibraltar: A combined experimental and numerical modeling study, J. Geophys. Res., 114, C06002, doi:10.1029/2008JC005023.

Sánchez Román, A., J. García Lafuente, J. Delgado, J.C. Sánchez Garrido, and C. Naranjo (2012), Spatial and temporal variability of tidal flow in the Strait of Gibraltar, J. Mar. Sys., doi:10.1016/j.marsys.2012.02.011.

Sannino, G., A. Carillo, and V. Artale (2007), Three-layer view of transports and hydraulics in the Strait of Gibraltar: a three-dimensional model study, J. Geophys. Res., 112, C03010, doi:10.1029/2006JC003717.

Sannino G., L. Pratt, and A. Carillo, Hydraulic criticality of the exchange flow through the Strait of Gibraltar (2009), J. Phys. Oceanogr., 39 (11), 2779-2799, doi:10.1175/2009JPO4075.1.

Sanz, J. L., J. Acosta, M. Esteras, P. Herranz, C. Palomo, and N. Sandoval (1991), Prospección geofísica del Estrecho de Gibraltar (resultados del programa Hércules 1980–1983), Publicaciones Especiales Instituto Español Oceanografía, 7, 48 pp., Madrid (Spain), 1991.

Vázquez, A., M. Bruno, A. Izquierdo, D. Macías, and A. Ruiz-Cañavate (2008), Meteorologically forced subinertial flows and internal wave generation at the main sill of the Strait of Gibraltar, Deep-Sea Res. I, 55,1277-1283, doi:10.1016/j.dsr.2008.05.008

Vázquez, A., S. Flecha, M. Bruno, D. Macías, and G. Navarro (2009), Internal waves and short scale distribution patterns of chlorophyll in the Strait of Gibraltar and Alborán Sea, Geophys.Res. Lett., 36, L23601, doi:10.1029/2009GL040959.

Vlasenko, V., J.C. Sánchez-Garrido, N. Stashchuk, J. García-Lafuente, and M. Losada (2009), Three-dimensional evolution of large amplitude internal waves in the Strait of Gibraltar, J. Phys. Oceanogr., 39, 2230-2246, doi:10.1175/2009JPO4007.1.

Watson, G., and I.S. Robinson (1990), A study of internal waves propagation in the Strait of Gibraltar using shore-based radar images, J. Phys. Oceanogr., 20, 374–395.

Wesson, J., and M. Gregg (1994), Mixing at Camarinal sill in the Strait of Gibraltar. J. Geophys. Res., 99 (C5), 9847–9878, doi:10.1029/94JC00256.

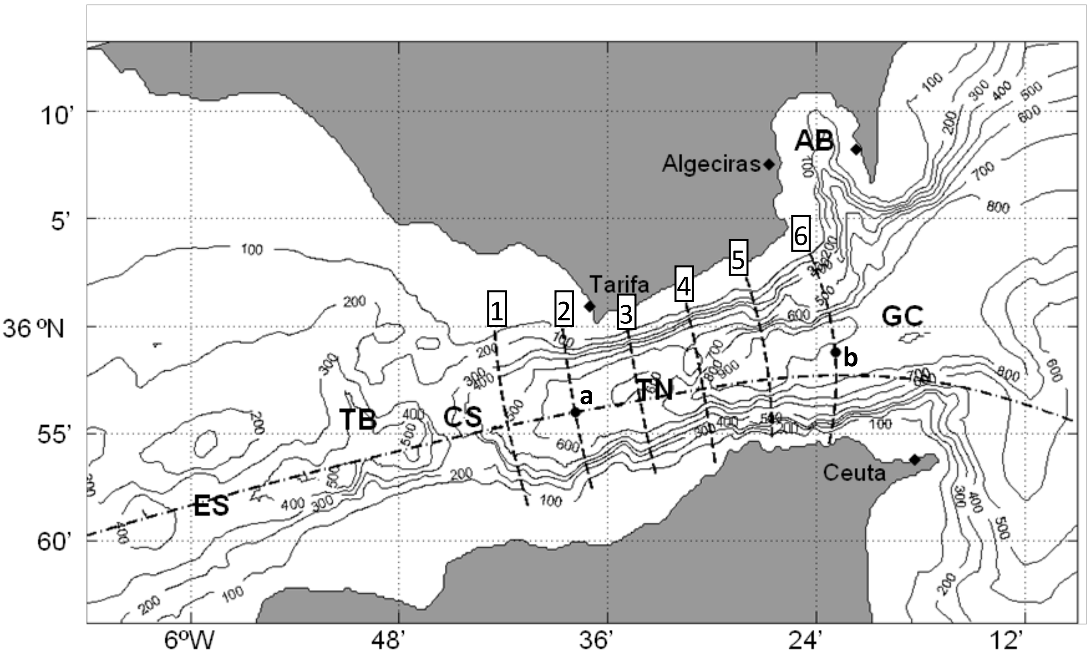

Figure 1.- Map of the Strait of Gibraltar showing the main topographic features mentioned in the text. From left to right they are: ES, Espartel Sill; TB, Tangier Basin; CS, Camarinal sill; TN, Tarifa Narrows; AB, Algeciras Bay; GC, Gibraltar-Ceuta section (the eastern exit of the Strait). Labeled dashed lines are cross-sections used to carry out different computations (see text). The dot-dashed line represents the along strait main section used to present flows and other parameters in succesive figures.

La línea de puntos y trazos representa la sección principal a lo largo estrecho utilizado para presentar los flujos y otros parámetros en las figuras adicionales

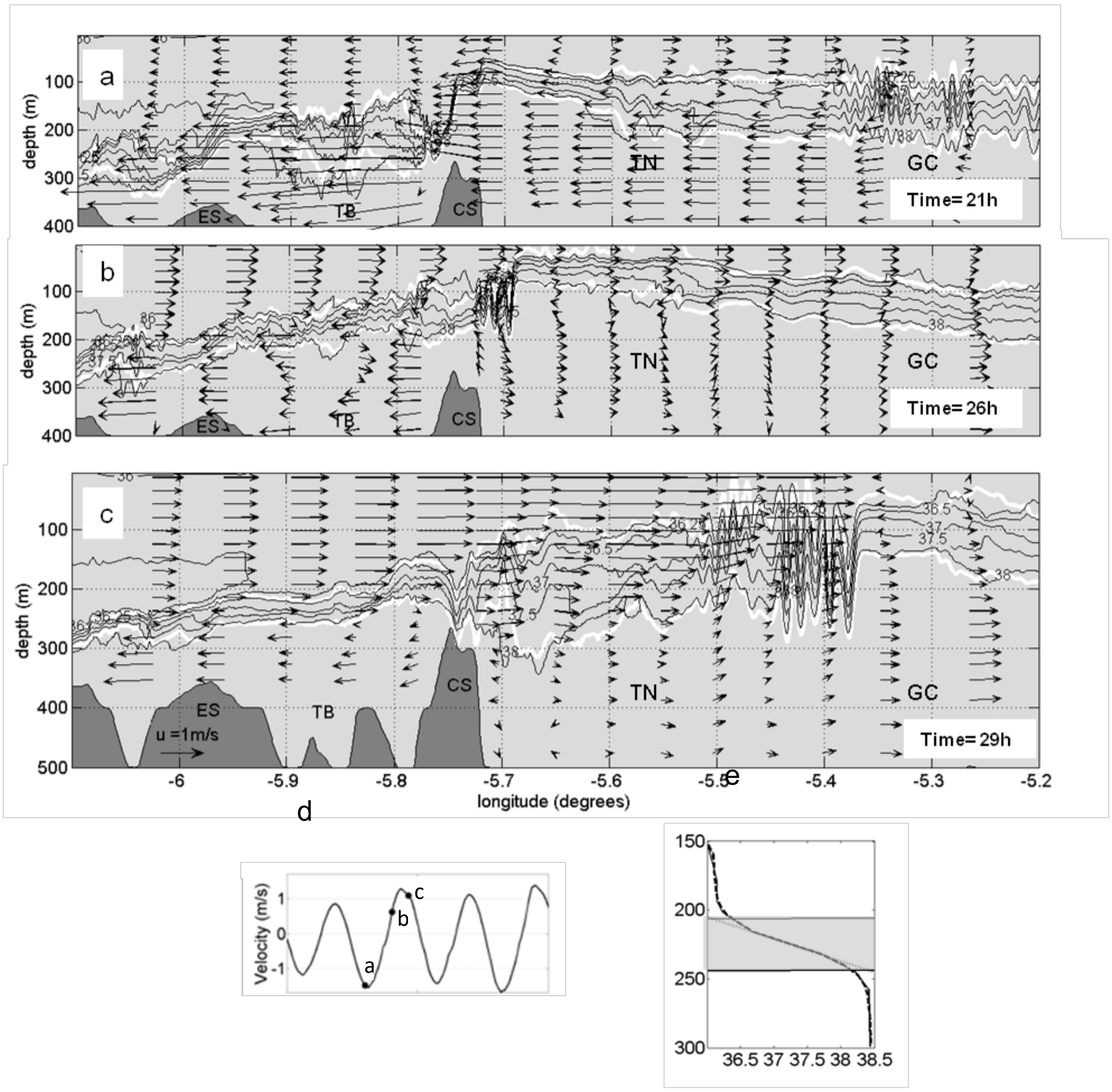

Figure 2.- Panels a), b) and c): Along-strait velocity field (velocity scale in panel c) in the vertical section indicated in Figure 1 at three different moments of the tidal cycle (panel d). Black lines are isohalines of S=36.0 (only visible on the far left of the panels), 36.25, 36.5, 37, 37.5 and 38. Thick white lines are the boundaries of the interface layer defined according to the explanation in the text. Panel d) is the barotropic tidal current at CS section and shows the moments of the snapshots a), b) and c). Panel e) shows a salinity profile to illustrate the method to determine the boundaries of the interface layer, which is shown in shading.

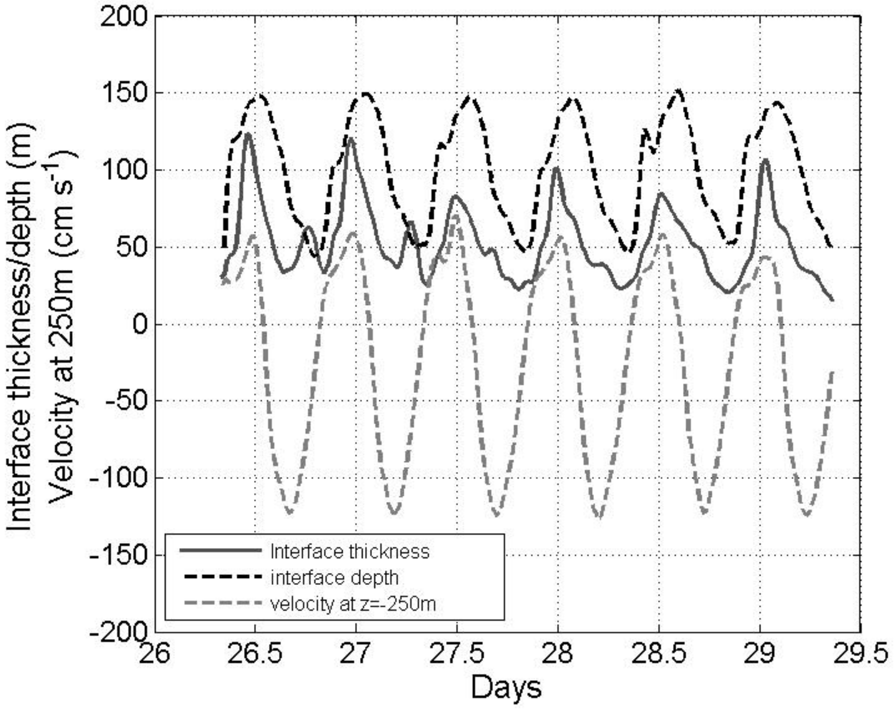

Figure 3.- Solid line: vertical distance separating S=37.7 and S=36.8 isohalines used here as a proxi of the interface thickness. Black dashed line: depth of the S=36.8 isohaline, a proxi of the interface depth. Grey dashed line: along-strait velocity at 250m depth, used as a proxi of the barotropic tide (see text for more details). The three variables correspond to the site "a" showed in Figure 1 and have been smoothed by a gaussian filter of cutoff frequency 1 cph in order to remove the high frequency fluctuations associated with the LAIWs.

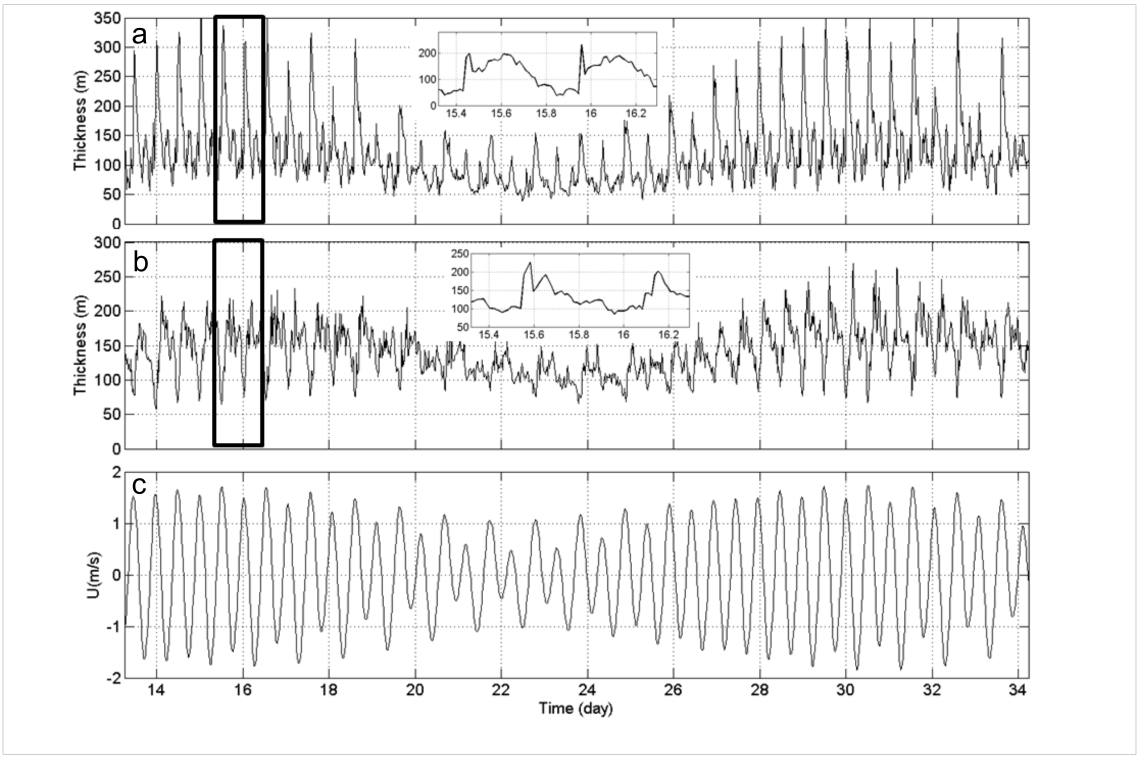

Figure 4.- Interface thickness at the sites "a" (panel a) and "b" (panel b) indicated in Figure 1. The inserts enlarge the portion of the record marked by the thick rectangles to illustrate the largely non-sinusoidal shape of the periodic oscillation, which appears more deformed to the east . Panel c) is the barotropic tidal current at CS section.

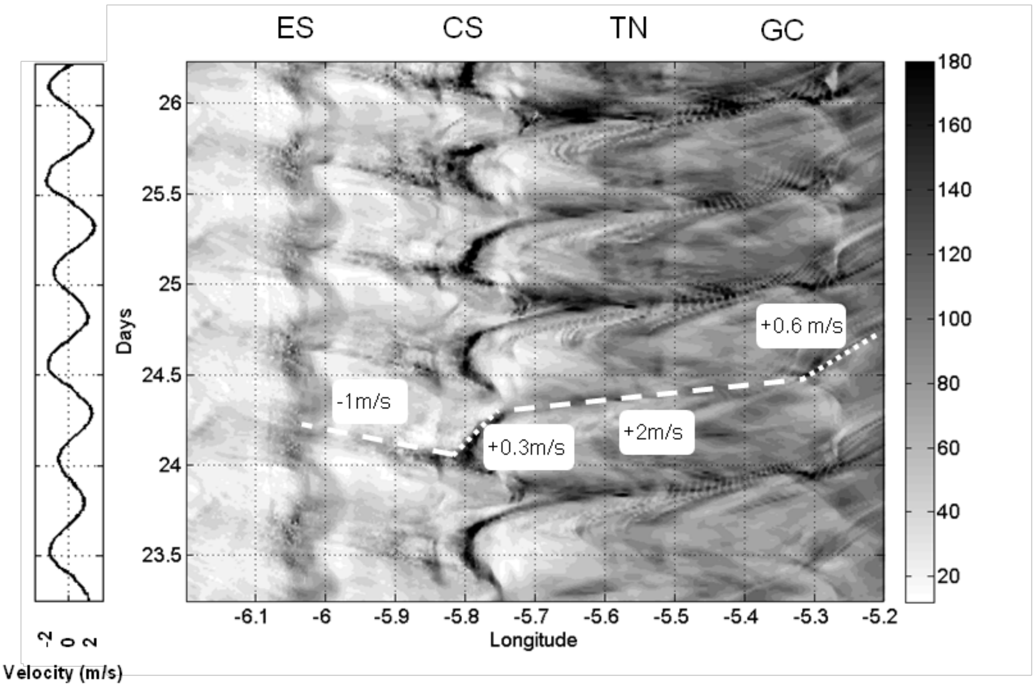

Figure 5.- Time-spatial evolution of the interface layer thickness (meters) along the central axis of the Strait. Labels on the top indicate the location of the main topographic features (see Figure 1). The straight dashed white lines and the numbers beside specify the propagation speed of the layer thickness, which changes from one region to the other. Barotropic tidal current at CS is shown in the left panel .

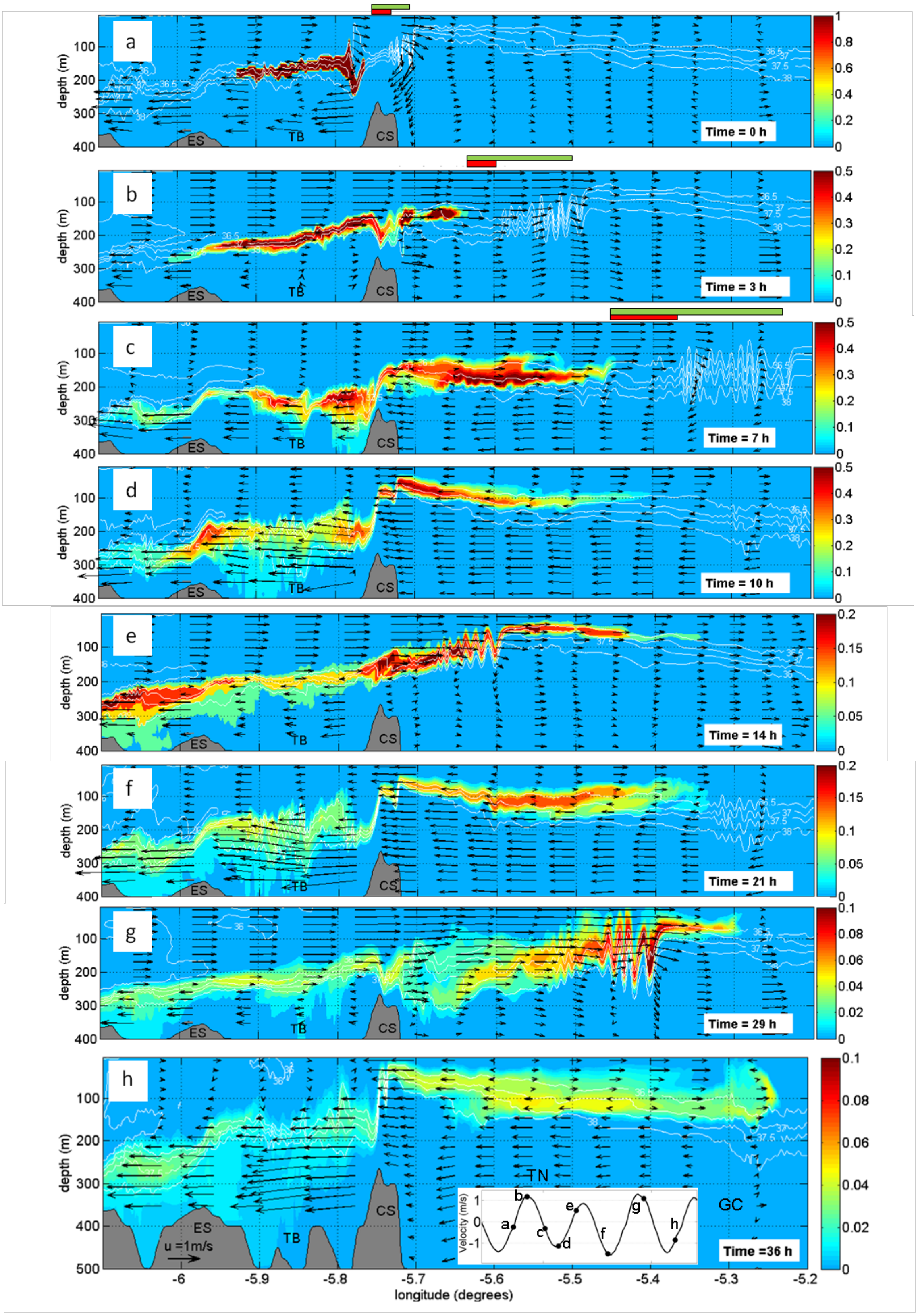

Figure 6.- Time evolution of the concentration of a passive tracer injected in TB at *t*=0 (panel a). Arrows indicate the along-strait velocity (scale in panel h) and white lines are isohalines S=36 to S=38.0 with ΔS=0.5. Insert in panel h) illustrates the barotropic tidal current in each panel. Green and red shaded rectangles on top of panels a), b) and c) indicate the distance between the nose of the tracer and the front and rear of the LAIWs train, respectively.

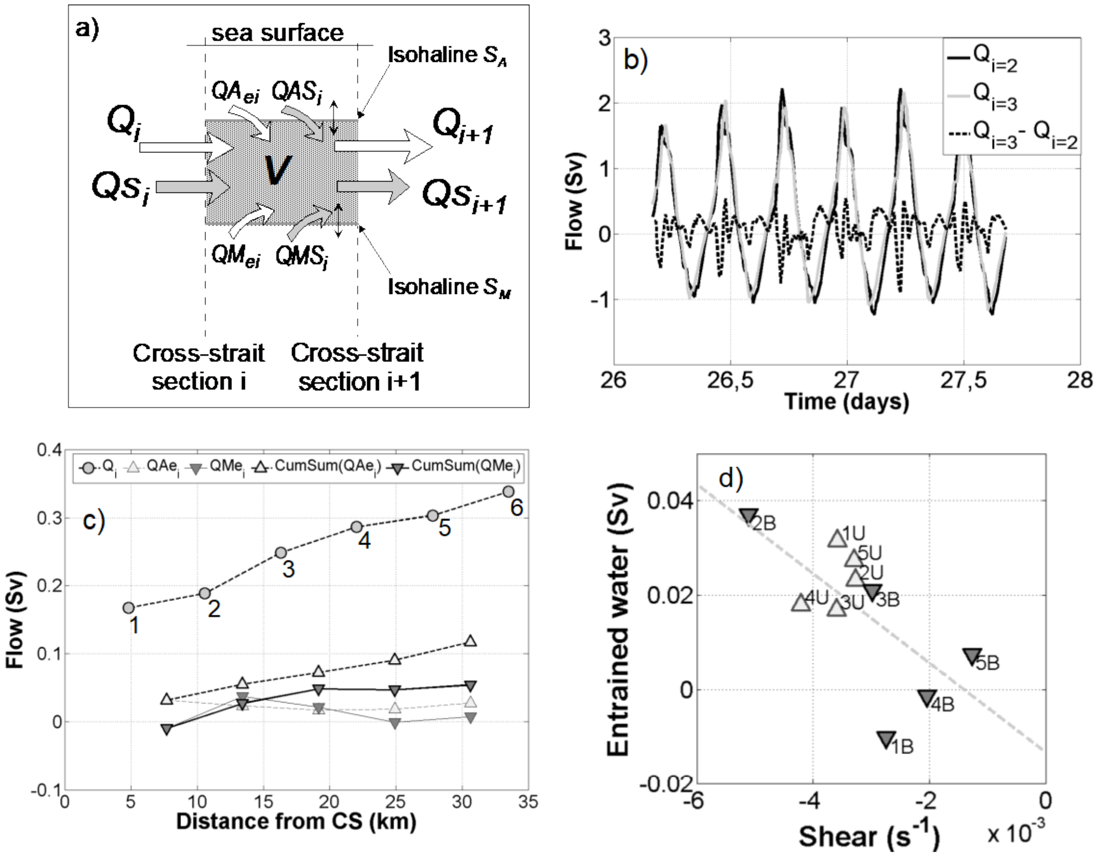

Figure 7.- a) Sketch of the volume control used to estimate the entrained water into the interface layer. Cross-strait sections that closes the volume laterally will be identified with the sections shown in Figure 1. b) Instantaneous interface flow through vertical cross-sections *i*=2 and *i*=3 and their difference, which is indicative of the rate of volume change *dV/dt* in box 2, the box defined by these sections. c) Tide-average flow through the six cross-sections of Figure 1 (filled circles), locally entrained water from above (QAe_i, light grey triangles) and below (QMe_i, light grey, inverted triangles) and cumulated entrained water from above (black triangles) and below (black inverted triangles). d) Scatter plot of entrained water versus mean vertical shear (see text). Open and inverted filled triangles correspond to water entrained from above and below (i.e., QAe_i and QMe_i), respectively. Labels beside symbols indicate the different boxes (i=1..5) for water entrained from above (U) or below (B). The straight dashed line is the linear fitting whose slope is -9.5 Sv.s.

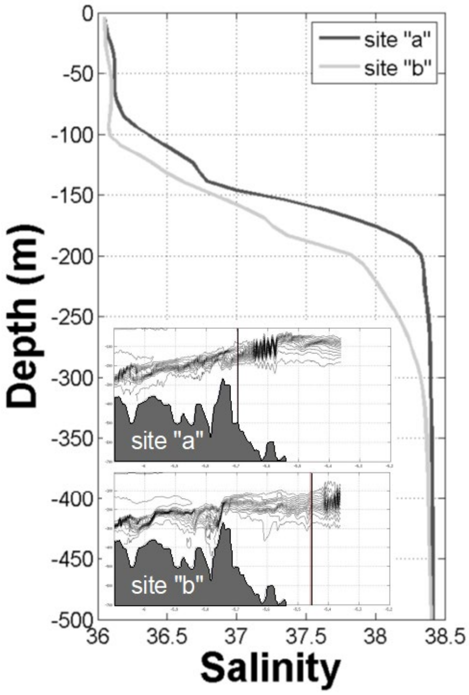

Figure 8.- Salinity profiles at sites “a” (black line) and “b” (grey line) showed by the vertical lines in the inserted along-strait sections (see also Figure 1) shortly after the local passing of the LAIWs train. Salinity gradient is smoother at site “b” suggesting the direct effect of the LAIWs train on mixing.

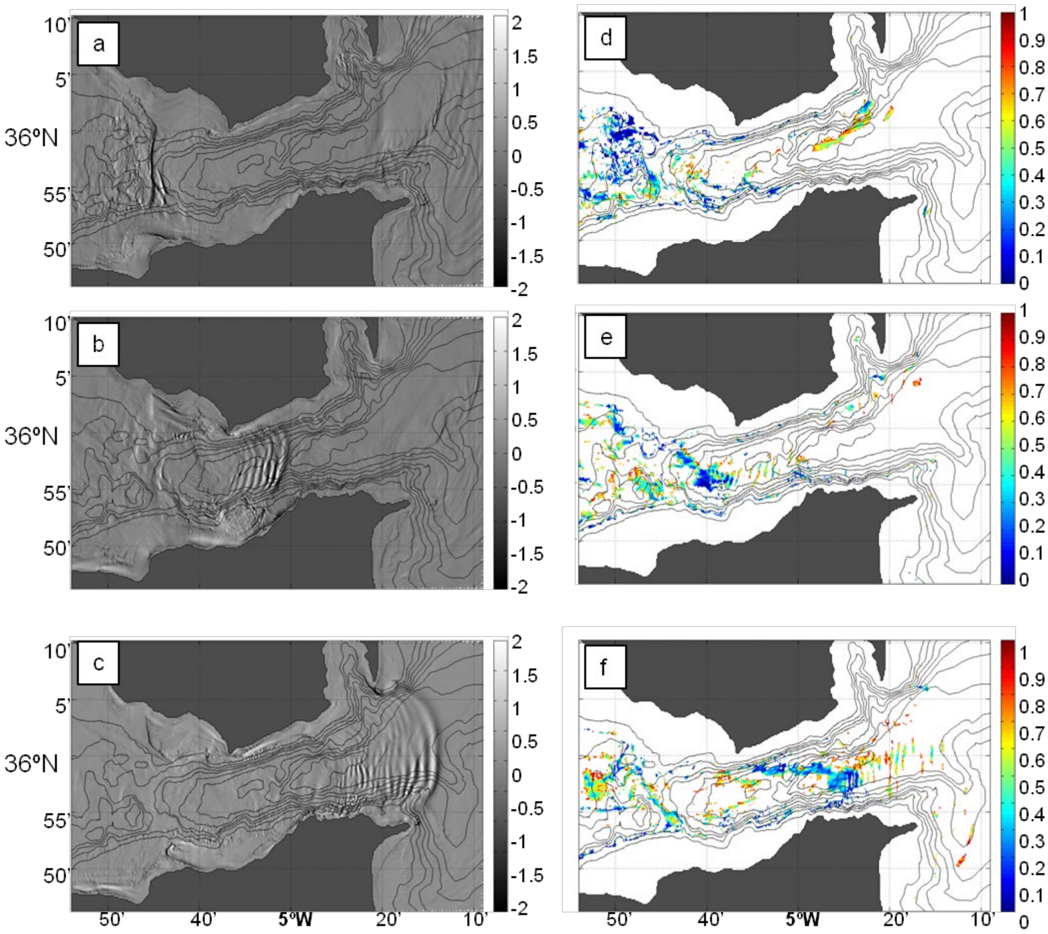

Figure 9.- Left panels: three different moments of the generation and propagation of LAIWs, which are depicted by the divergence of the surface velocity. Panel a) shows the signature of the internal hydraulic jump downstream of CS, and panels b) and c) show the LAIWs train passing off Tarifa and about leaving the Strait, respectively, after the release of the jump. Right panels: Richardson *Ri* number computed at 160m depth at the same moment as in the corresponding left panel. Notice the very low values at the rear of the LAIWs packet in panels e) and f) and the extended low values all over TB in panel d) coinciding with the formation of the hydraulic jump.

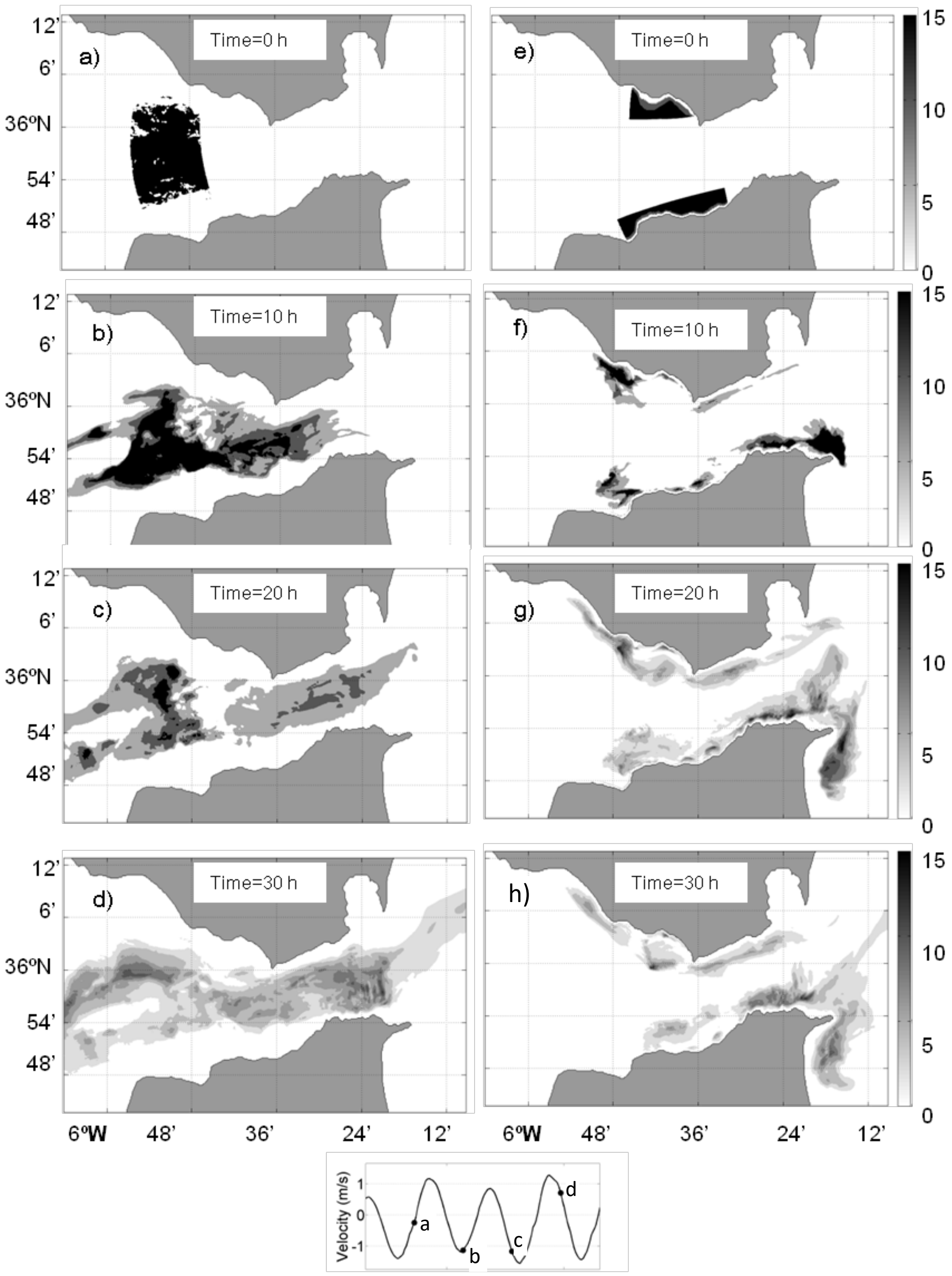

Figure 10.- Time evolution of a passive tracer injected initially at the central part of the strait in TB (panel a) and in coastal waters (panel e). Panels b) to d) show the subsequent evolution of the vertically integrated concentration at t=10h, 20h, and 30h, respectively, for the initial situation (*t*=0) shown in panel a). Panels f) to h) do the same for the case of the initial situation (*t*=0) shown in e). The bottom panel shows the barotropic tidal current at CS and indicates the four instants of the different snapshots.

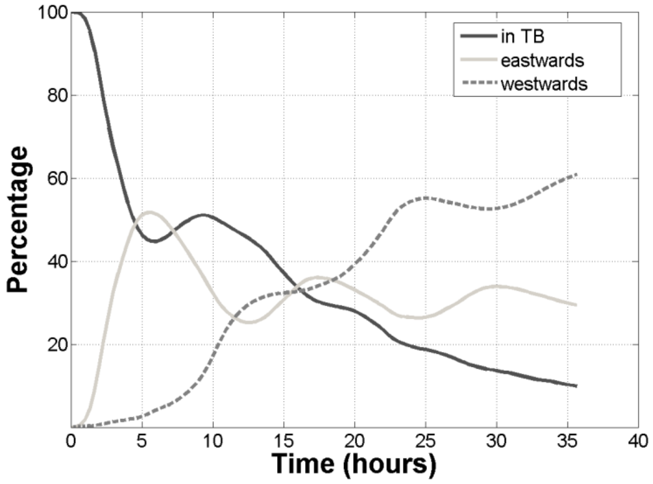

Figure 11.- Time evolution of tracer concentration (percentage). Black line is the tracer that remains in Tangier basin, grey solid and dashed lines represent the tracer advected eastwards over CS and westwards over ES, respectively.